Chapter 5 -- Numerical Verification

5.1 Overview

The governing equations for the axisymmetric response of a shell of revolution under axisymmetric loading have been manipulated into a first-order state vector form, which constitutes a two-point boundary value problem with separated boundary conditions. As such, the problem is well posed for solution by a shooting technique. In this work, we have undertaken to apply just such a technique. In particular, we have used a modified form of the "stabilized marching method" (Ascher, Mattheij and Russell, 1988).

In this chapter, verification of the results obtained by shooting is presented. Some verification has previously been offered (Steinbrink and Johnson, (1997)): the shooting code has been shown to accurately predict (a) membrane response under internal pressure, (b) torsional response and (c) bending response for an isotropic spherical shell, and to correctly show that membrane response should not be expected for orthotropic shells. In addition, this same reference also points out a certain advantage of the shooting technique over the displacement-based finite element method: higher accuracy in calculation of the transverse shear stress resultants.

Additional features of the shooting code not previously verified include incorporation of elastic boundary conditions, orthotropic dome properties, non-spherical geometry and geometrically nonlinear response. Verification of these features is obtained by comparison of shooting results to results of a finite element analysis using the code STAGS (Brogan, et al, 1996). We here present four test cases. Verification Case I represents an analysis of the geometrically linear response of an orthotropic dome joined to a quasi-isotropic right circular cylinder under internal pressure. There is a polar opening in the dome which is closed by an isotropic plate. Verification Case II is an examination of the geometrically nonlinear response of two different laminates for spherical domes under internal pressure, with clamped edges. Next, in Verification Case III we examine the linear and geometrically nonlinear response of ellipsoidal domes under internal pressure, with clamped edges. Finally, in Verification Case IV we expand upon the case of an isotropic spherical dome with clamped edges and internal ring stiffeners, first reported in Steinbrink and Johnson (1997).

Material properties for Verification Cases I-III are:

$$E_1 = 22.5Msi \qquad E_2 = 1.755Msi \qquad E_3 = 1.755Msi$$
$$G_{12} = 0.638Msi \qquad G_{13} = 0.638Msi \qquad G_{23} = 0.464Msi$$
$$\nu_{12} = 0.248 \qquad \nu_{13} = 0.248 \qquad \nu_{23} = 0.458$$

with a ply thickness of 0.00625 inches. These material properties are chosen to represent a generic material system, and this ply thickness was chosen for convenience. For the cover plate of Verification Case I and for the dome of Verification Case IV, we use material properties of a certain type of Aluminum, those being given by $E = 10.5Msi$, $\nu = 0.33$. While these material parameters may not represent any particular material or material system, they should suffice for the intended purpose of numerical verification. Definition of the dependent variables plotted here are given in Figs. 3.1 and 3.2.

5.2 Verification Case I: Spherical dome capping a right circular cylinder under internal pressure, with cover plate

For this case, the cylinder and cover plate are represented by equivalent sets of stress resultants. The stress resultants are linearly related to displacements at the joints made with the dome, and to the internal pressure. The linear relationship is determined by the unit displacement method. A model of the cylinder is created having all displacements fixed to zero at the remote end (that is, the end away from the joint,) and allowing a single unit-valued displacement at the local end (i.e., the joint end). Shooting is performed with pressure set to zero and the calculated resultants at the local end define a column of the matrix *K* correspondent to the applied displacement. For example, if the displacement vector chosen is $\Delta = [0, 1, 0, 0, 0]^T$, then the calculated resultant vector at the local end may be taken as the second column of *K*. After all five columns of *K* have been evaluated by the unit displacement method, we next set the remote end boundary conditions to match those which are expected in service. For this problem, we expect a membrane response far from the joint, so we take the boundary conditions at the remote end to be $u = 0$, $v = 0$, $Q_1 = 0$, $M_{11} = 0$, $M_{12} = 0$. We clamp the local end, and specify a unit-valued pressure. The calculated local-end resultants are saved as a vector $\hat{v}$. Then the cylinder may

be expected to provide an equivalent elastic stress resultant vector $\vec{\sigma}_e$ to the dome edge, defined by

$$\vec{\sigma}_e = [K]\vec{\Delta} + p\vec{v}$$

where $\vec{\Delta} = [u, v, w, \varphi_1, \varphi_2]^T$, the reference surface displacement vector. A similar analysis is performed for the cover plate. For the purpose of this verification case, the dome is modeled as less-than-hemispherical, with an included angle α in the range $30° \le \alpha \le 80°$, with α as defined in Fig. 5.1, below. The wall of the cylinder is a quasi-isotropic laminate, $[\pm 45,0,90]_s$, the dome wall is a $[\pm 30]_{2s}$ layup, and the cover plate is isotropic (Aluminum) of thickness 0.1 inch. An internal pressure of 20 pounds per square inch is applied.

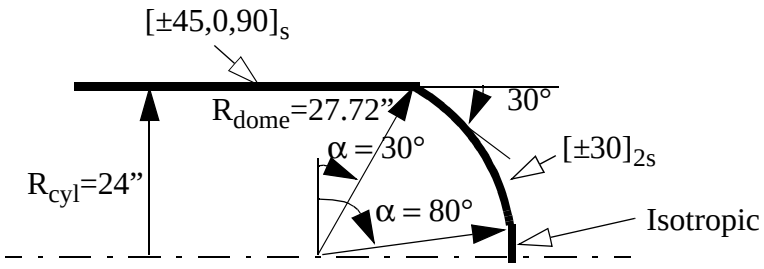

Fig. 5.1 Verification Case I: Spherical Dome Capping a Right Circular Cylinder, with Cover Plate

For the finite element analysis, the cylinder/dome/plate combination is modeled as a whole. The boundary conditions are as follows: at the remote end of the cylinder the normal displacement is free, and all other displacements are fixed to zero. The same conditions are applied at the apex end of the plate. The finite element analysis uses the STAGS element 480, which is a nine-noded Assumed Natural Strain element, incorporating transverse shear deformation effects. The cylinder is modeled as 24” in length, with 50 elements along the cylinder meridian; the dome is modeled with 100 elements along the meridian, and the cover plate uses 20 elements. In the circumferential direction, elements of the cylinder are of length 0.05 inches, which equals the shell thickness, and elements of the dome and plate are taken to subtend an arc of 0.0133°, which

provides an arc length of 0.05 inches at the joint of the dome and cylinder. This small circumferential length was chosen in order that the model would approximate an analysis along a meridian, thus allowing direct comparison to results of the shooting code. Boundary conditions on the circumferential faces of the FEM model were taken to provide axial symmetry of response: circumferential displacement, rotation about the meridional axis and rotation about the normal to the shell surface are set to zero, and all other displacements are free.

The significant displacements for this test case are shown in Figs. 5.2, 5.3 and 5.4, with the translational displacements normalized by the shell wall thickness. For this test case, both the FEM and the shooting code predict near-zero displacement in the circumferential direction and near-zero rotation about the meridional axis, throughout the solution domain. The agreement between the two analyses is quite good.

The results of the shooting method and the finite element analysis also agree well for the stress resultants and stress couples, with one notable exception: the in-plane shear stress resultant N_{12}. More will be said on this discrepancy later.

Fig. 5.2 Scaled Meridional Displacement, Case I

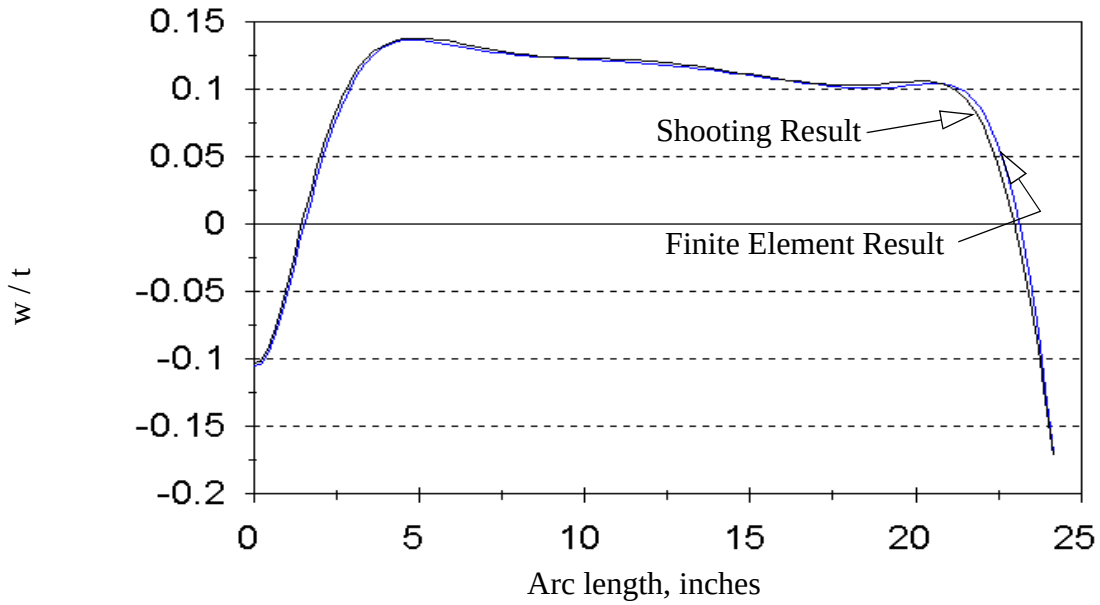

Fig. 5.3 Scaled Normal Displacement, Case I

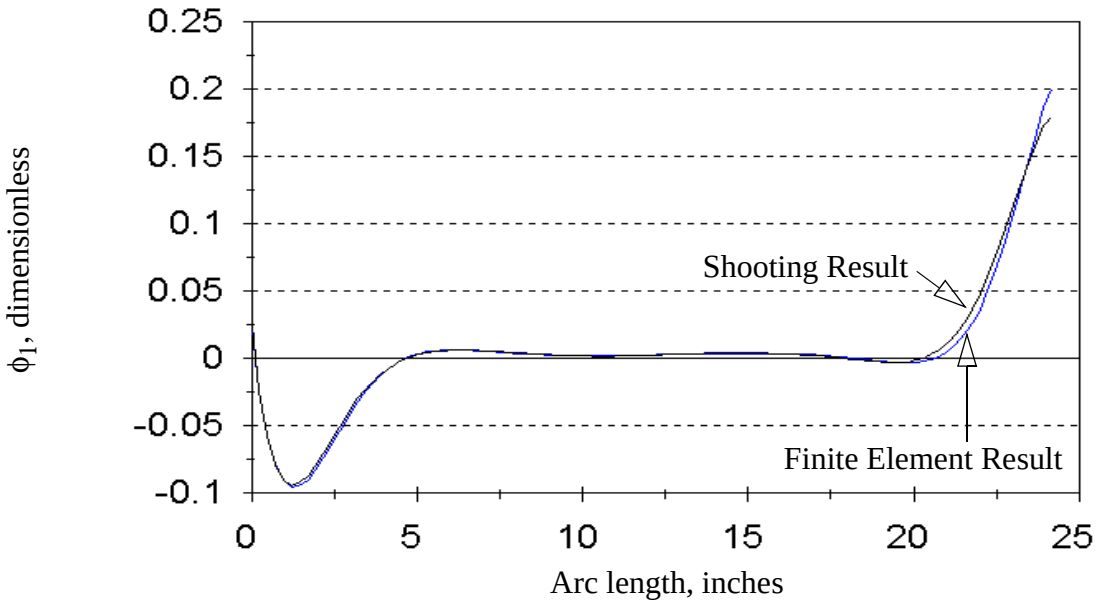

Fig. 5.4 Rotation About Circumferential Axis, Case I

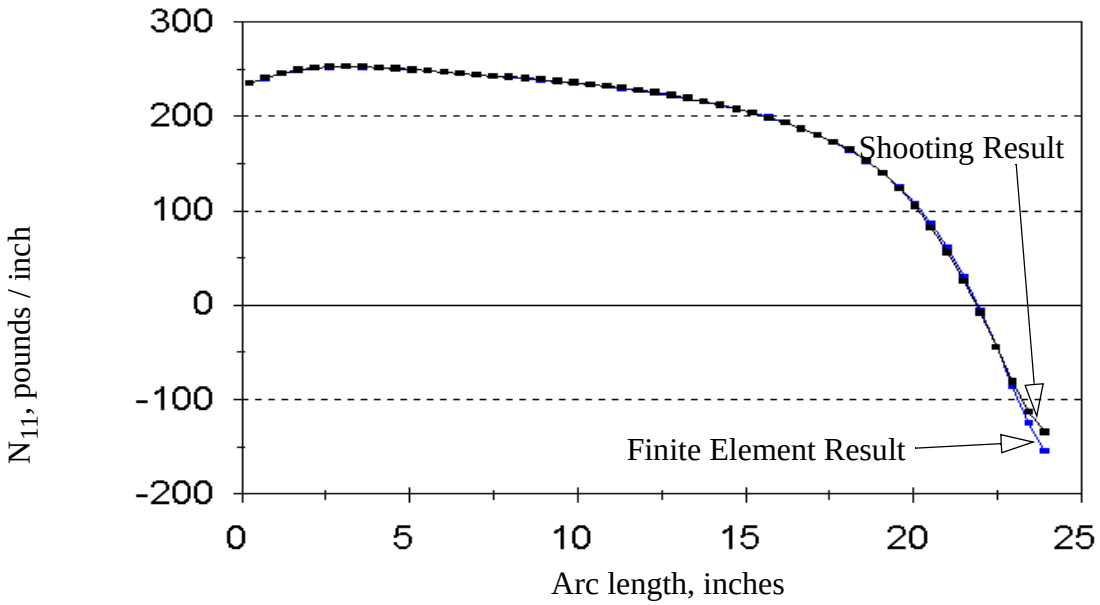

Fig. 5.5 Meridional Stress Resultant, Case I

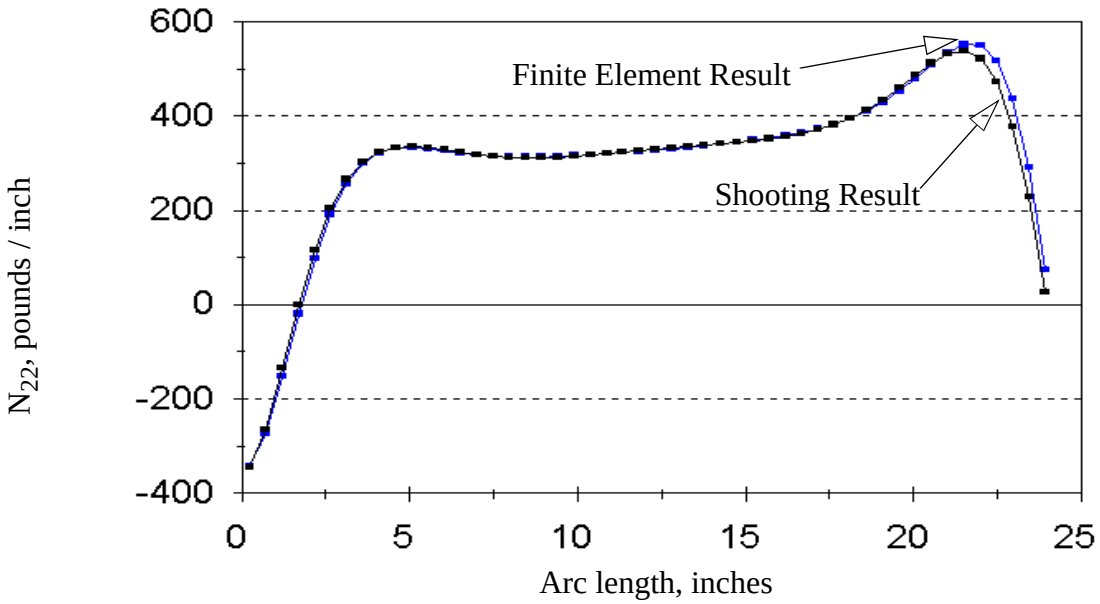

Fig. 5.6 Circumferential Stress Resultant, Case I

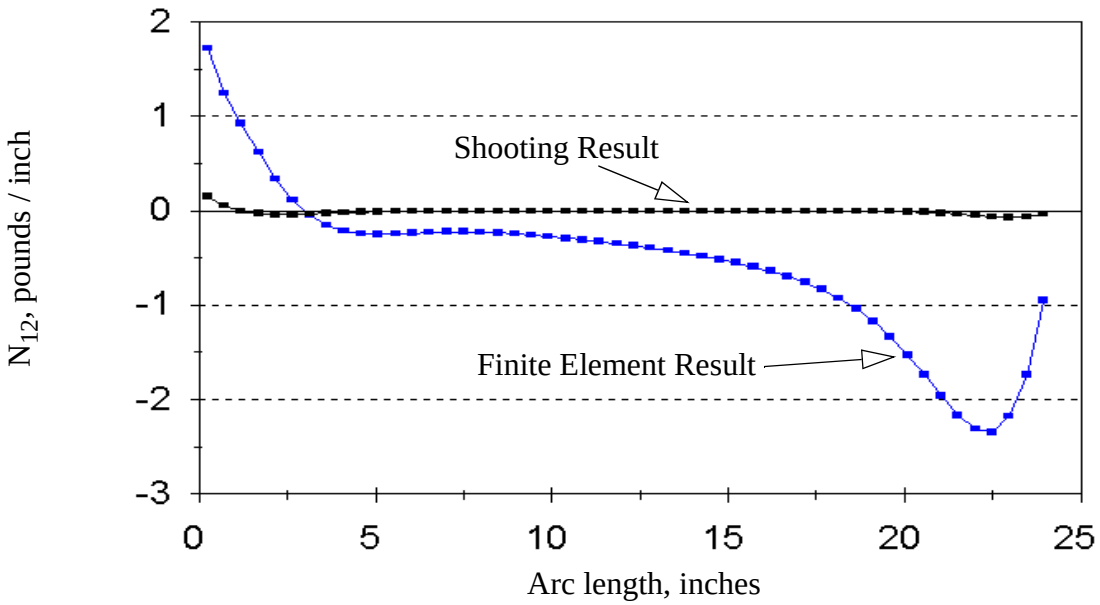

Fig. 5.7 In-plane Shear Stress Resultant, Case I

Fig. 5.8 Meridional Stress Couple, Case I

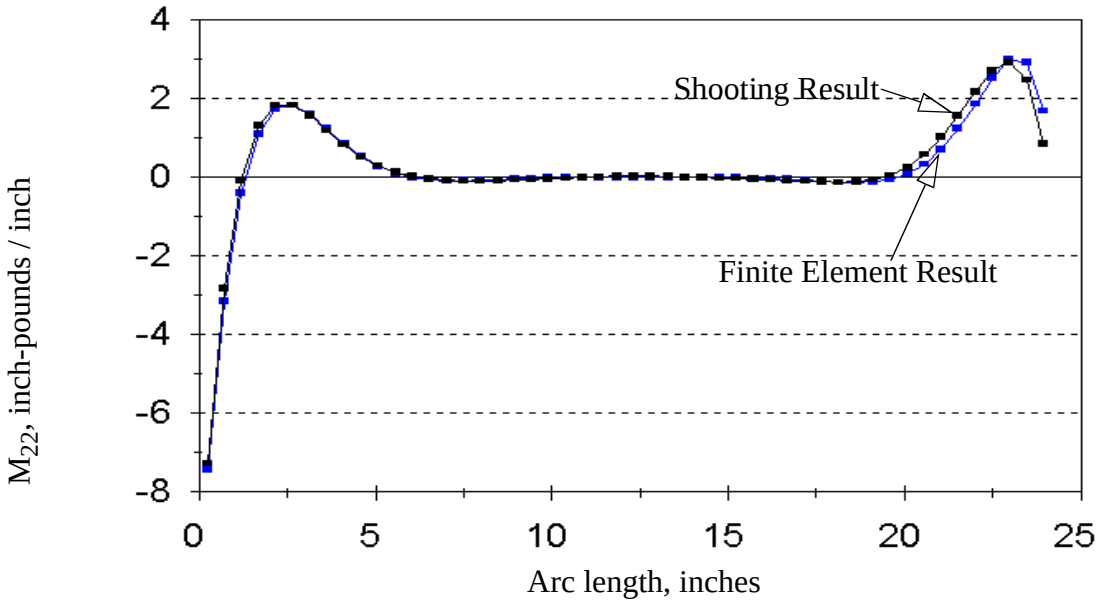

Fig. 5.9 Circumferential Stress Couple, Case I

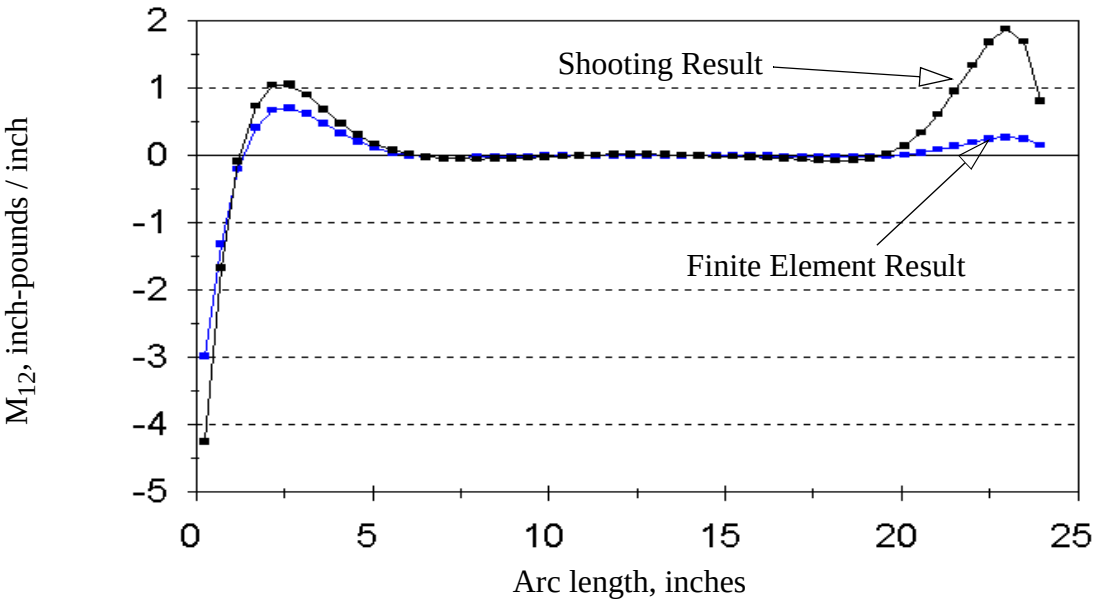

Fig. 5.10 In-plane Stress Couple, Case I

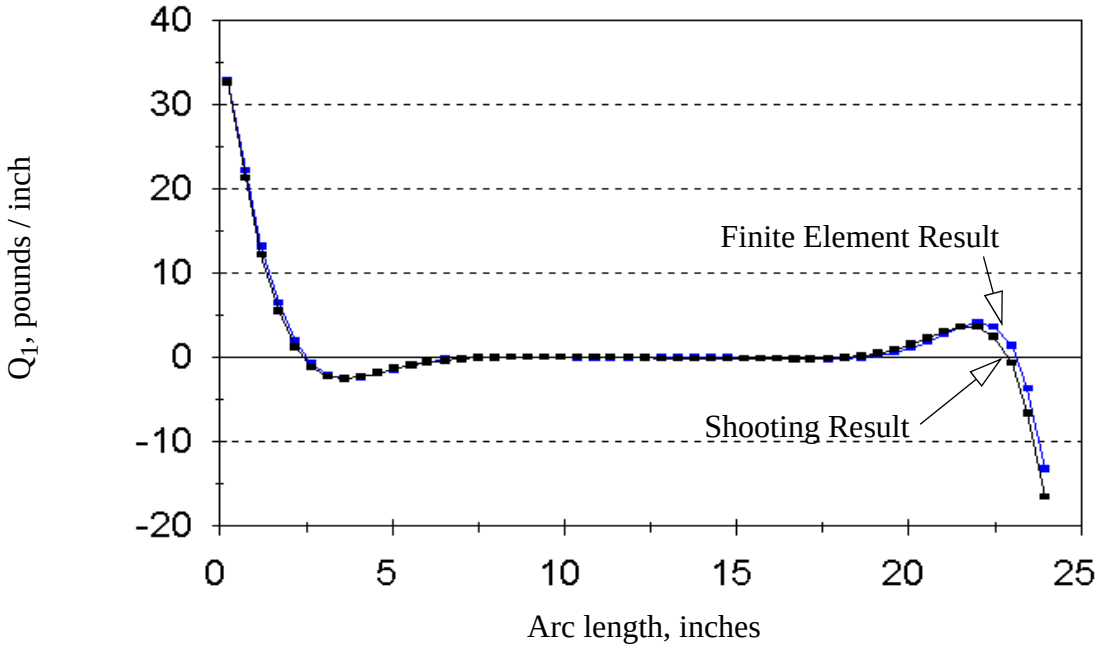

Fig. 5.11 Transverse Shear Stress Resultant on Meridional Face, Case I

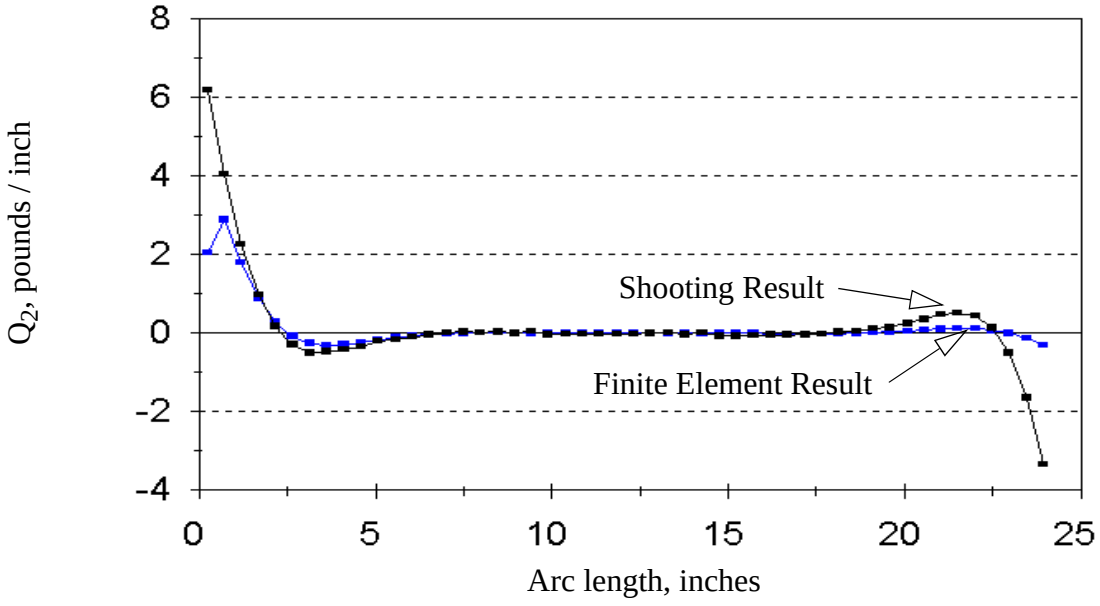

Fig. 5.12 Transverse Shear Stress Resultant on Circumferential Face, Case I

As previously mentioned, there is large disagreement between the results generated using the finite element code STAGS and the results of the shooting code, for the in-plane shear stress resultant N_{12}. This disagreement is readily seen by an examination of Fig. 5.7. The cause for this discrepancy is unknown, but it appears to be a problem with STAGS. The argument for this latest assertion is this: It is known that for the special case of an isotropic or quasi-isotropic spherical shell, the equations of equilibrium and the strain-displacement relations of linear shell theory split such that the problem decouples into a purely torsional and a purely torsionless case. In this case, loading under internal pressure (only) with no applied torsional displacements should lead to $N_{12} \equiv 0$. The results of a shooting analysis conform closely to this theoretical requirement, whereas the results obtained from STAGS do not. See Fig. 5.13 for results of the isotropic test case; similar results were seen for the quasi-isotropic test case.

For these tests, the ends of the dome are taken to be rigidly fixed. The STAGS model and the shooting analysis both take 101 evenly spaced nodes (shooting points). The finite element model has three nodes in the circumferential direction, spanning 0.5 degrees altogether. Initially, a quarter-symmetry model of the dome was used, but it was found that taking a much narrower circumferential strip reduced the error. The STAGS model uses element 480, with symmetry boundary conditions on the circumferential faces. The model is of an almost hemispherical dome, $0° \le \alpha \le 80°$ (with angular measure as implicitly defined in Fig. 5.1), radius R = 24 inches, thickness of 0.05 inches, and pressure of 60 psi.

We conclude from these simple tests that there is a problem with STAGS. The erroneous output from STAGS has been shown to be greatly reduced (though not adequately eliminated) by decreasing the element length in the circumferential direction, further casting doubt on the finite element analysis results. Furthermore, this discrepancy is further reduced when the analysis is run with STAGS element 410, a four-noded quadrilateral shell element.

While the above arguments cannot demonstrate accuracy of the shooting code for the in-plane shear stress resultant, there is no reason to disbelieve the shooting results, particularly since all other comparisons to the FEM are quite good.

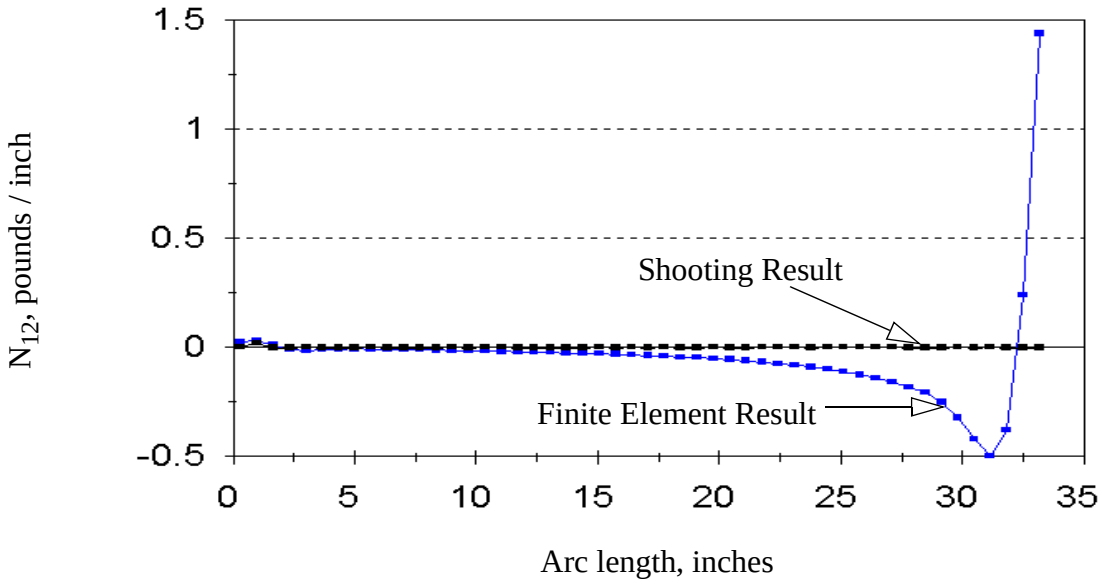

Fig. 5.13 In-plane Shear Stress Resultant for Isotropic, Spherical Dome with Clamped Ends

5.3 Verification Case II: Geometrically nonlinear analysis of spherical domes under internal pressure

For this test case, we have taken a fixed set of dome geometric and loading parameters, which are: constant radius of 24", pressure p = 60 psi, clamped at both edges. The loading is taken to be hydrostatic, and comparison is again made to results obtained from the finite element code STAGS. The nonlinear analyses were performed beginning with a linear analysis at 50% load, followed by nonlinear analyses at 50%, 75%, and 100% loading. Two test configurations are included here, which differ only in the laminate layup of the dome. The first of these configurations is a quasi-isotropic $[\pm 45,0,90]_s$ layup, and the second is a $[\pm 45,0_2]_s$ layup, which has a preferential stiffness in the meridional direction. In addition to the comparison of results for geometrically nonlinear analysis, the figures given here also include the results of geometrically linear analysis, generated by the shooting code. Some results from the quasi-isotropic test case are omitted here for brevity: the significant displacements are given, and nothing else. As may be seen by examination of Figs. 5.17 - 5.24, the comparisons for the meridionally stiff case are quite good, and sufficient in themselves to show correctness of the shooting results. Results of the quasi-isotropic case are included only as a matter of interest, to help illustrate the level of signifi-

cance of the geometric nonlinearities included.

Figs. 5.14 - 5.16 depict the meridional and normal displacements (scaled by the wall thickness) and the rotation about the circumferential axis, respectively, for the quasi-isotropic dome. The agreement between the results of the shooting analysis and the FEM analysis is good, particularly for the normal displacement and the rotation. The numeric results for meridional displacement compare less perfectly, but it seems likely that refinement of the load path (i.e., use of more load steps) would bring the results into closer agreement. It may be noted that the maximum normal displacement is rather large, compared to the wall thickness, in violation of one of the assumptions of the linear analysis. A geometrically nonlinear analysis is thus seen to be appropriate for these shells.

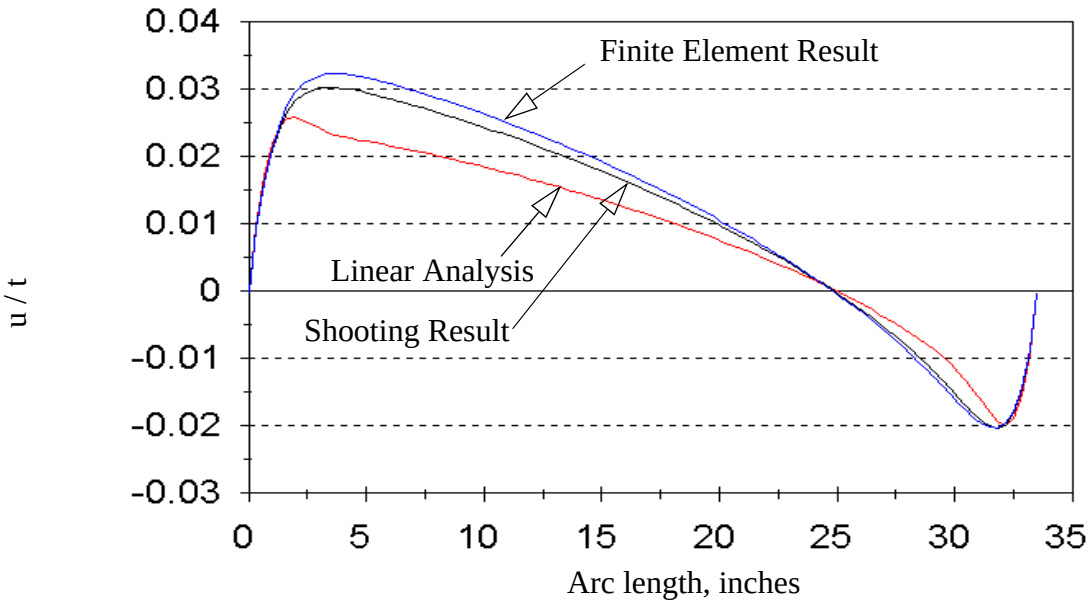

Fig. 5.14 Scaled Meridional Displacement, Case II (Quasi-isotropic)

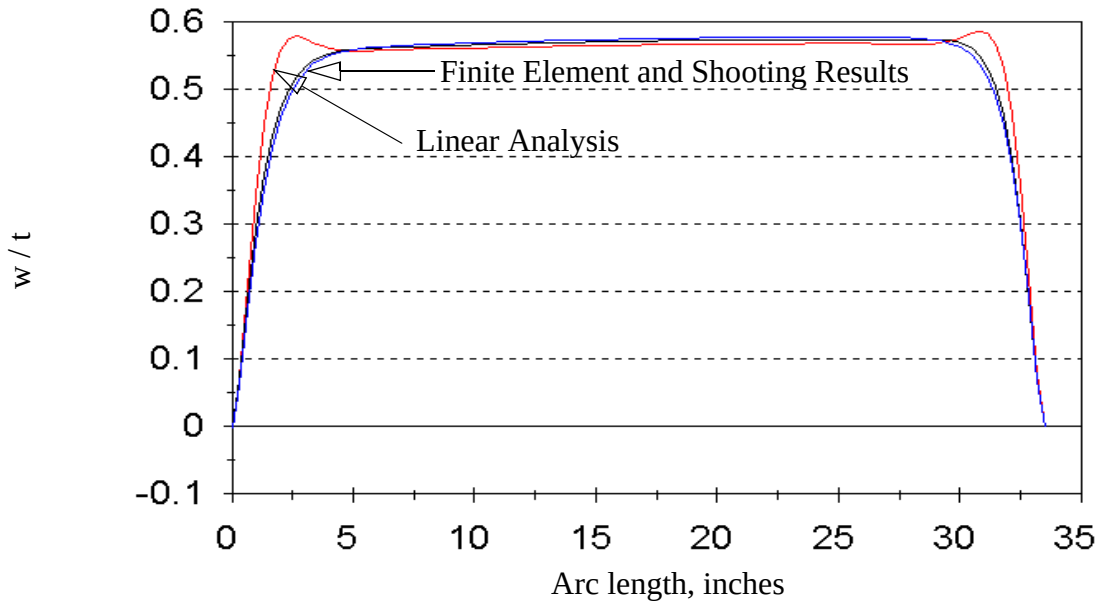

Fig. 5.15 Scaled Normal Displacement, Case II (Quasi-isotropic)

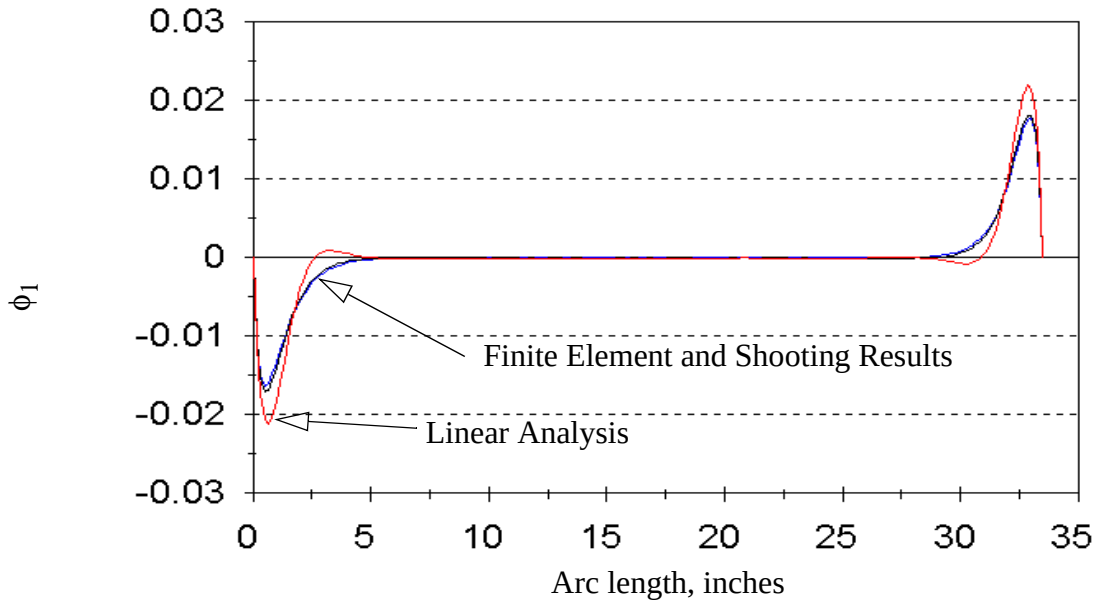

Fig. 5.16 Rotation About the Circumferential Axis, Case II (Quasi-isotropic)

The remaining figures of this section, Figs. 5.17 - 5.24, are for the $[\pm 45, 0_2]_s$ laminate. It may be seen that the agreement between the results of the shooting process and the results of the finite element analysis are good for all but the in-plane shear stress resultant N_{12}, and the transverse shear stress resultant Q_1. It was previously noted that STAGS element 480 seems to have difficulty in calculation of the in-plane shear stress resultant -- the disagreement of the analyses in this variable is not surprising. The discrepancy in the transverse shear stress resultant requires further exploration, but may result from STAGS use of a shear correction factor, which is not incorporated into the shooting code. The transverse shear stress resultant calculated using STAGS element 410 does not differ significantly from that of element 480. It may be noted by an examination of Fig. 5.22 that the geometrically nonlinear analysis of STAGS produces nearly the same transverse shear stress resultant as the linear analysis by numerical integration. Recall also that the current method of analysis by numerical integration was prompted in part by a perceived shortcoming in the finite element method, when used to calculate the transverse shear stress resultants.

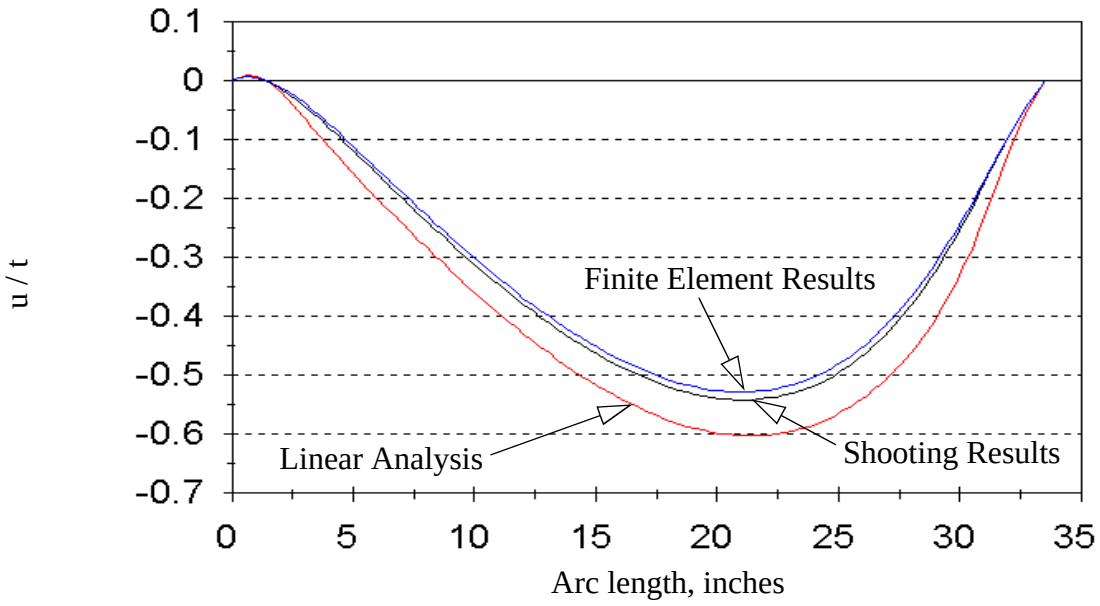

Fig. 5.17 Scaled Meridional Displacement, Case II (Meridionally Stiff)

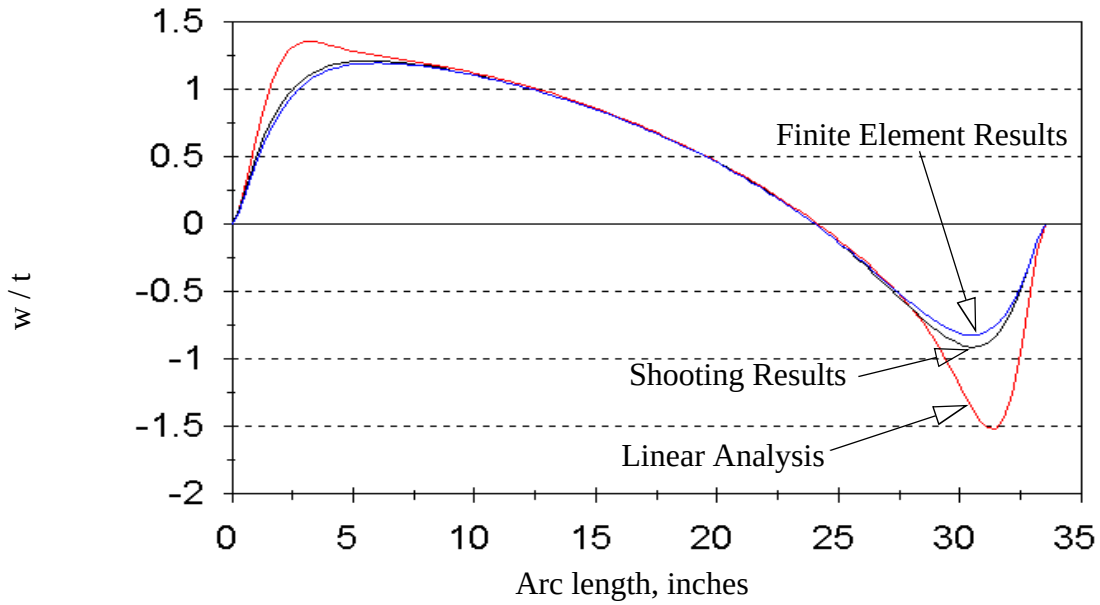

Fig. 5.18 Scaled Normal Displacement, Case II (Meridionally Stiff)

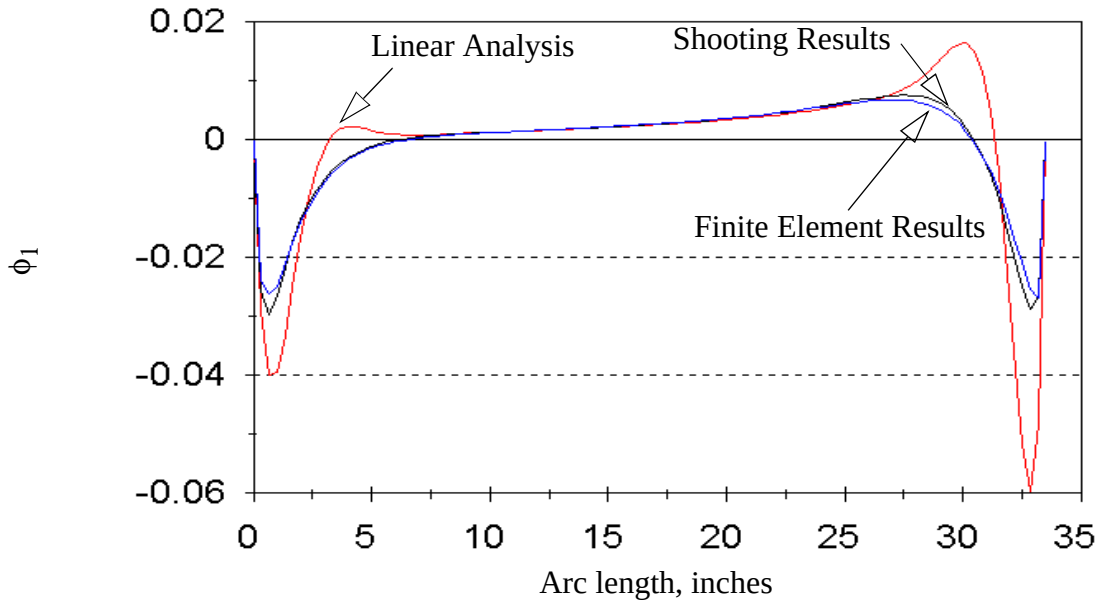

Fig. 5.19 Rotation About the Circumferential Axis, Case II (Meridionally Stiff)

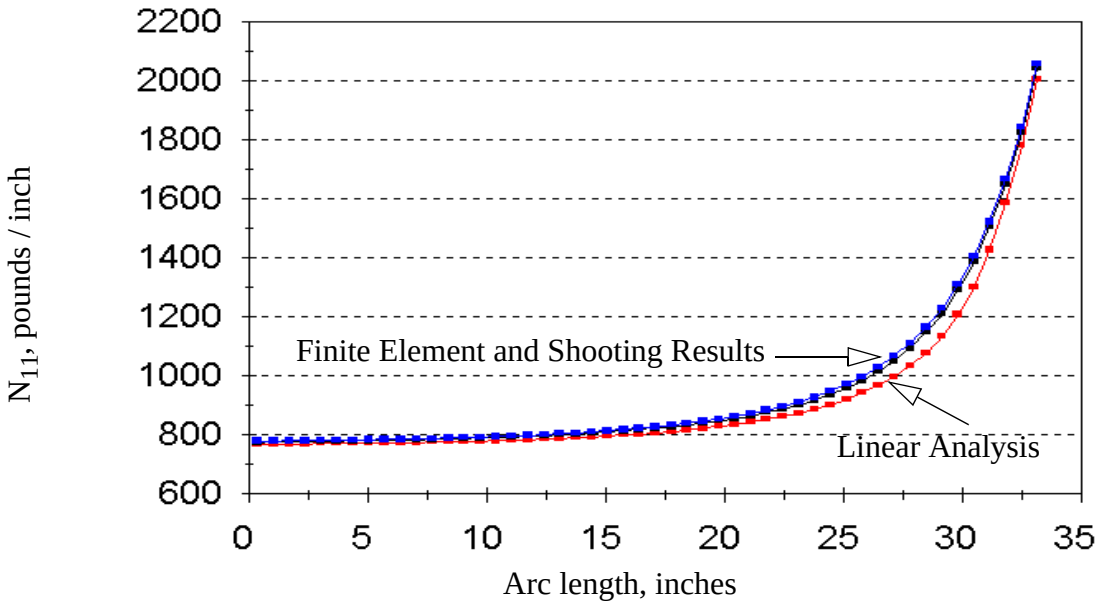

Fig. 5.20 Meridional Stress Resultant, Case II (Meridionally Stiff)

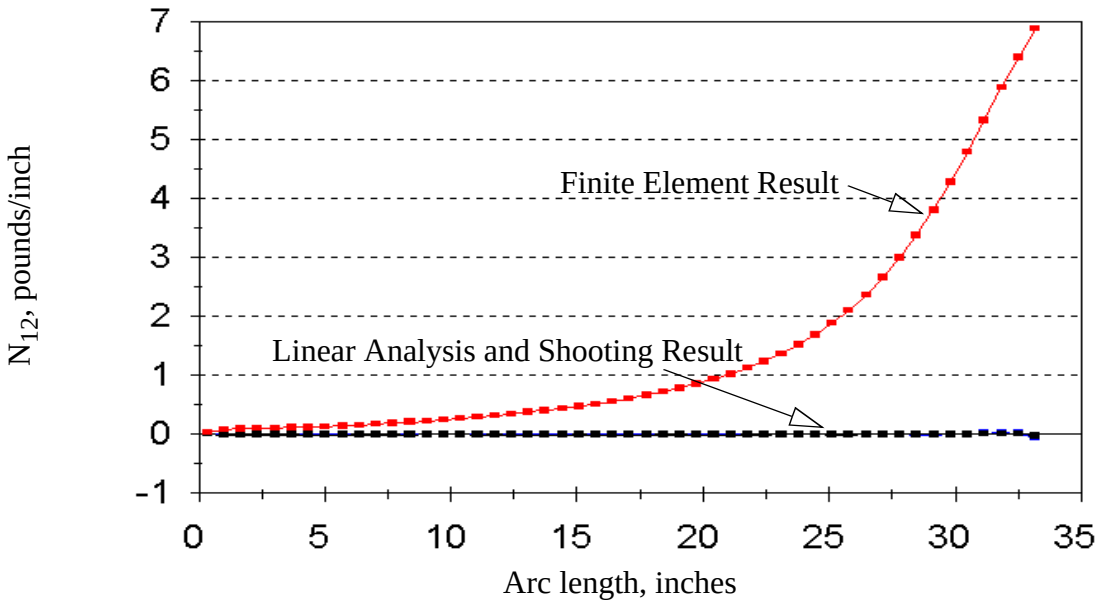

Fig. 5.21 In-plane Shear Stress Resultant, Case II (Meridionally Stiff)

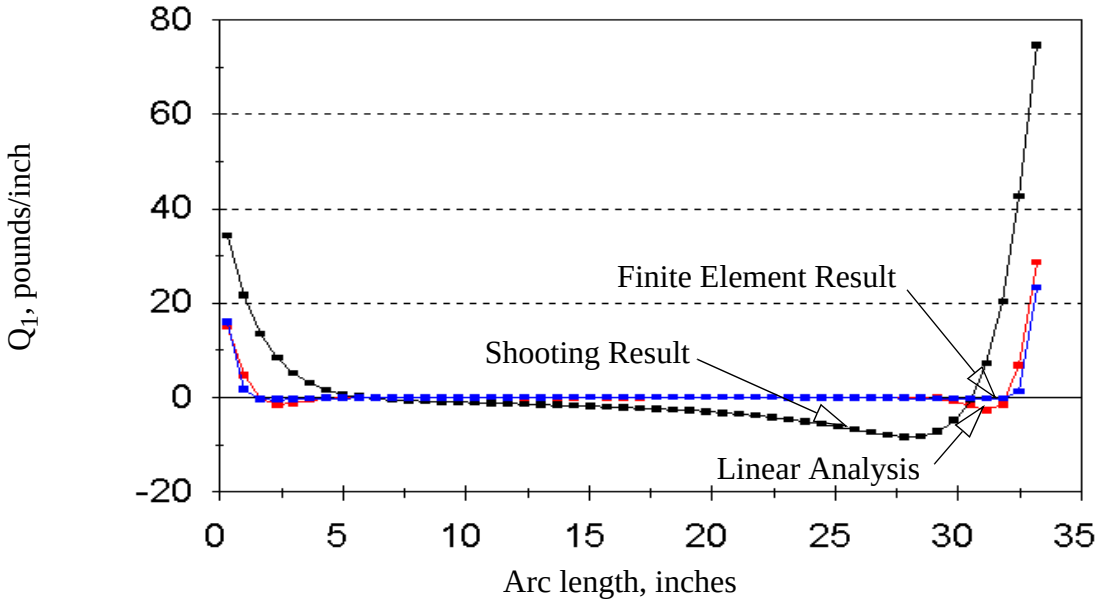

Fig. 5.22 Transverse Shear Stress Resultant, Case II (Meridionally Stiff)

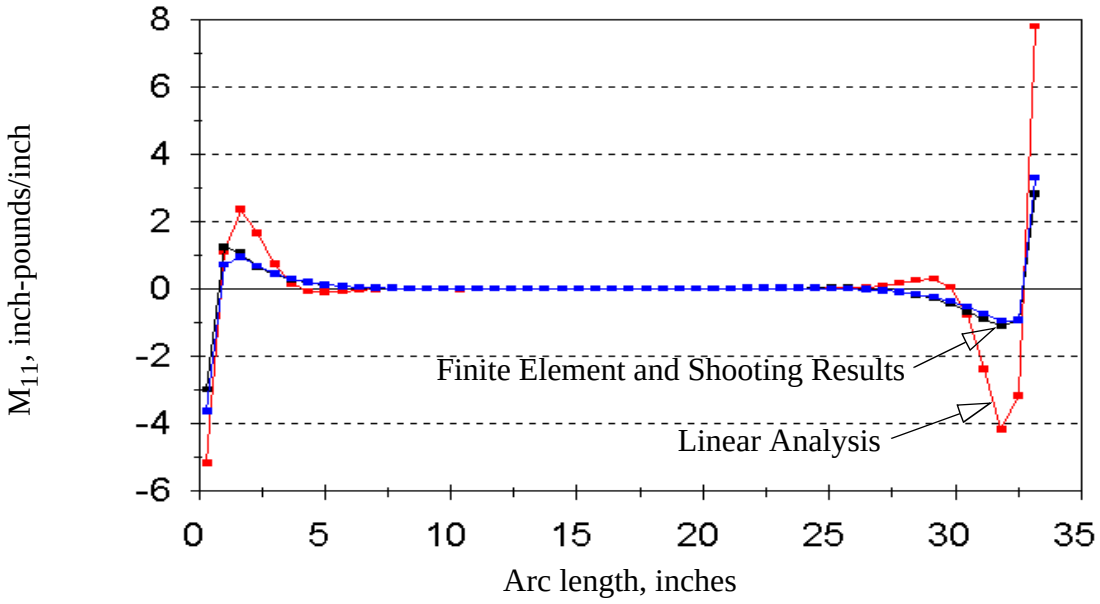

Fig. 5.23 Meridional Stress Couple, Case II (Meridionally Stiff)

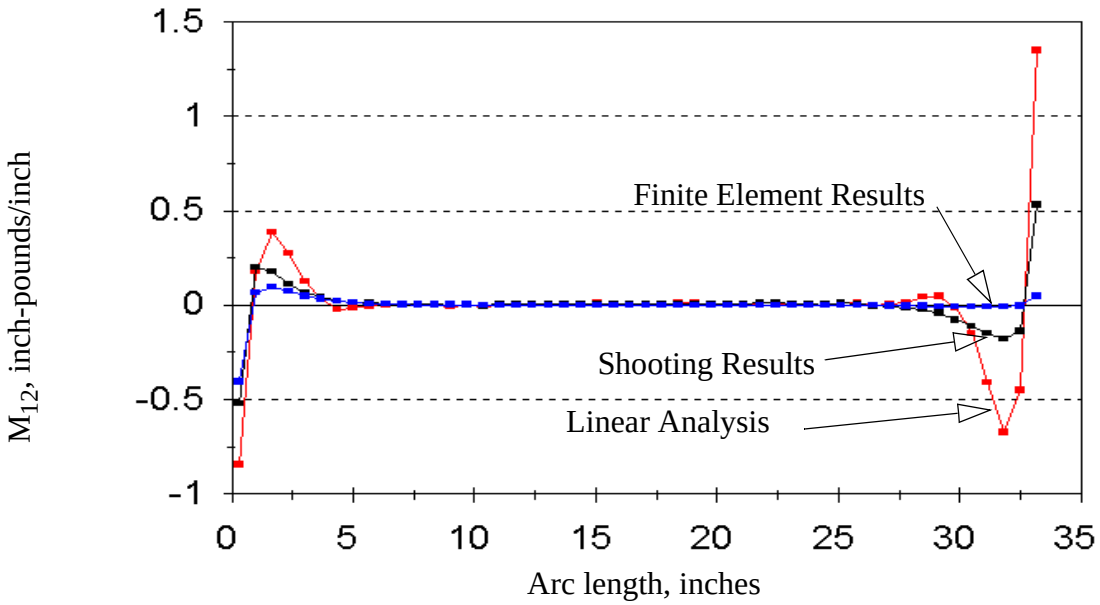

Fig. 5.24 In-plane Shear Stress Couple, Case II (Meridionally Stiff)

It may be interesting to note that geometric nonlinearities produce a softening effect in the quasi-isotropic laminate and a stiffening effect in the meridionally stiff case, as judged by comparison of Figs. 5.14 - 5.16 with their counterparts, Figs. 5.17 - 5.19.

5.4 Verification Case III: Analysis of ellipsoidal domes

The previously given verification studies have shown good agreement between the results of a finite element analysis and the results of a direct integration of the state vector equations, for spherical domes of various construction and with different boundary conditions. In this verification case, we examine the results for ellipsoidal domes, as shown in Fig. 5.25. We will take the major axis of the meridian to be directed perpendicular to the axis of revolution, and define the ellipticity *e* as the ratio of the semi-minor axis length to the semi-major axis length, with the minor axis parallel to the axis of revolution. The domes considered will be $[\pm 30]_{2s}$ laminates with clamped edges and included angle η in the range $0 \le \eta \le 80°$ under internal pressure of 60 psi. Comparison is made to the results of a finite element analysis using the code STAGS.

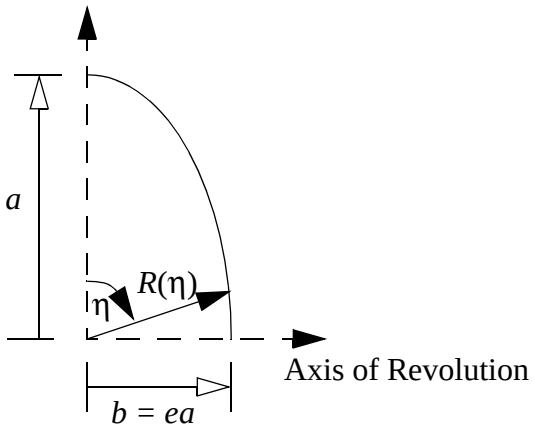

Fig. 5.25 Elliptical Meridian

As the first subcase for this verification test, Case IIIa, we consider a dome with ellipticity $e = 0.5$, and a semi-major axis length of 24 inches. A geometrically nonlinear analysis is performed, under hydrostatic pressure loading. A set of 101 shooting points is used for the integrations, with the points evenly spaced with respect to the included angle. The finite element model uses the same points for nodes along the meridian, and two nodes in the circumferential direction, spaced 0.5 degrees apart. The nodes are used to define a mesh of 100 four-noded quadrilateral shell elements. Clamped conditions are applied at the ends, with symmetry conditions applied on the circumferential faces. As in the previous cases, the meridional displacement and the normal displacement are scaled by the wall thickness. All other figures contain “raw” numbers. As may be noted by study of Figs. 5.26 - 5.28, the nonlinear analyses by numerical integration and by the finite element method do not match perfectly in the displacements; the agreement is, however, good, and the trends match perfectly. It may further be noted by study of Figs. 5.26 and 5.27 that the normal and meridional displacements are very large, compared to the shell wall thickness, and thus necessitate a geometrically nonlinear analysis.

Here again, it may be noted that the analysis by numerical integration and the analysis by the finite element method disagree in the in-plane shear stress resultant N_{12}, and in the transverse shear stress resultant Q_1.

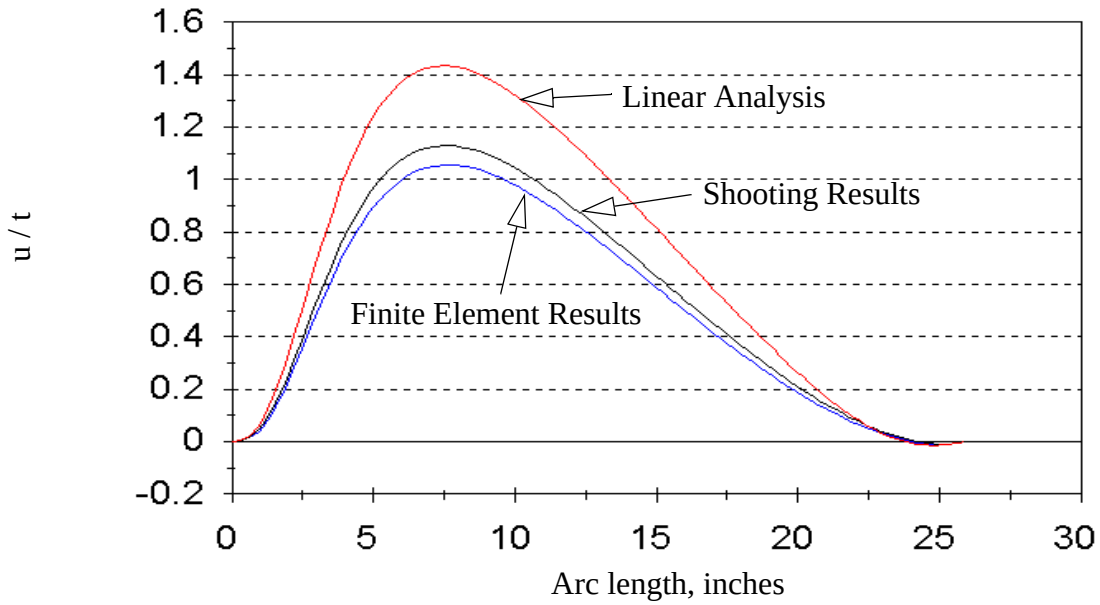

Fig. 5.26 Scaled Meridional Displacement, Case IIIa

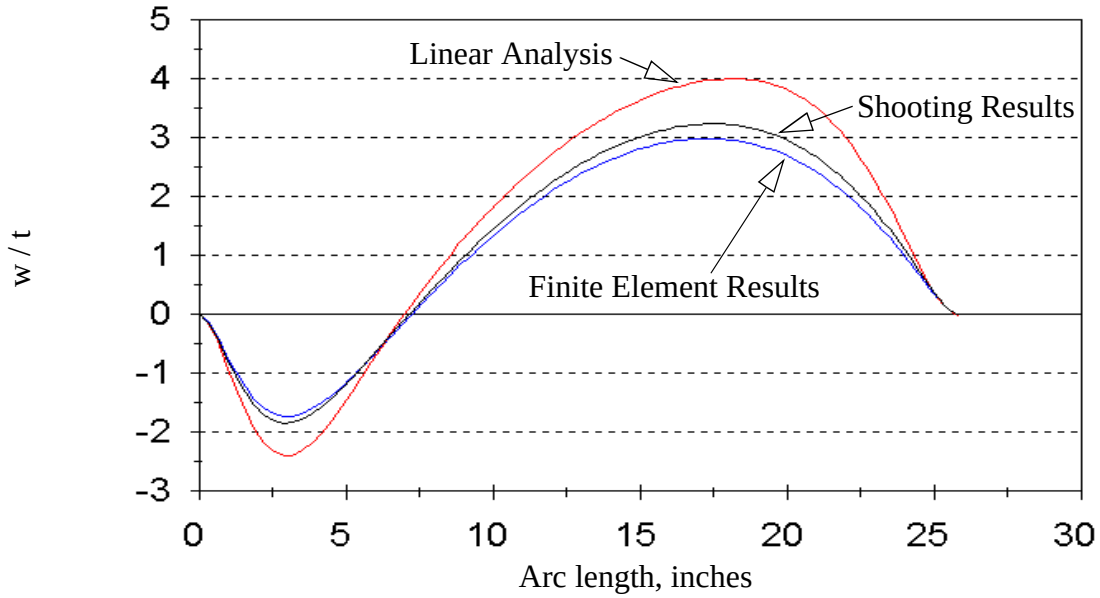

Fig. 5.27 Scaled Normal Displacement, Case IIIa

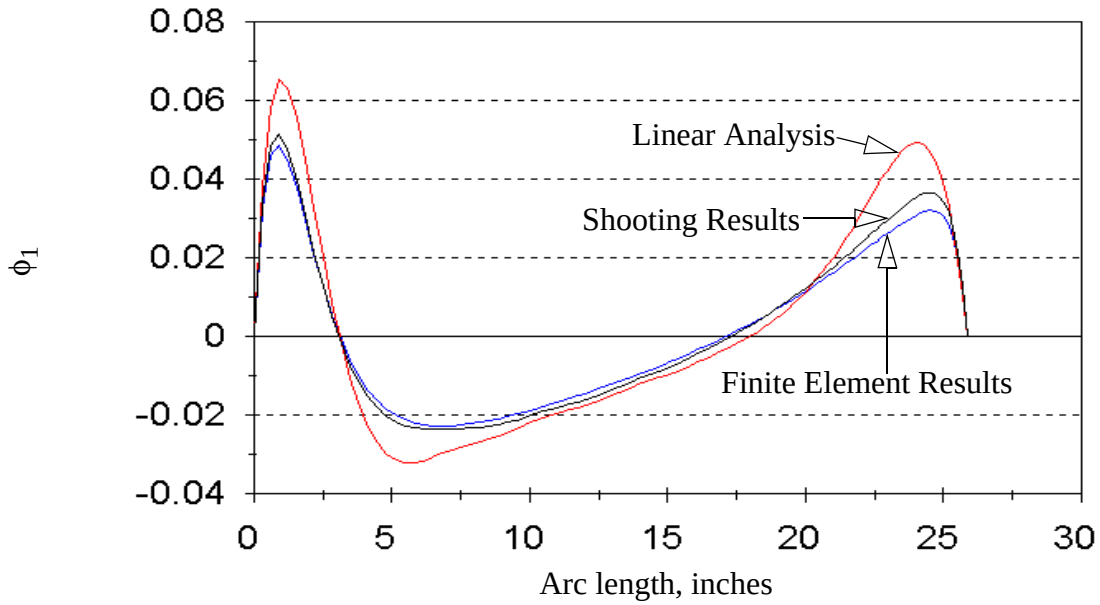

Fig. 5.28 Rotation About Circumferential Axis, Case IIIa

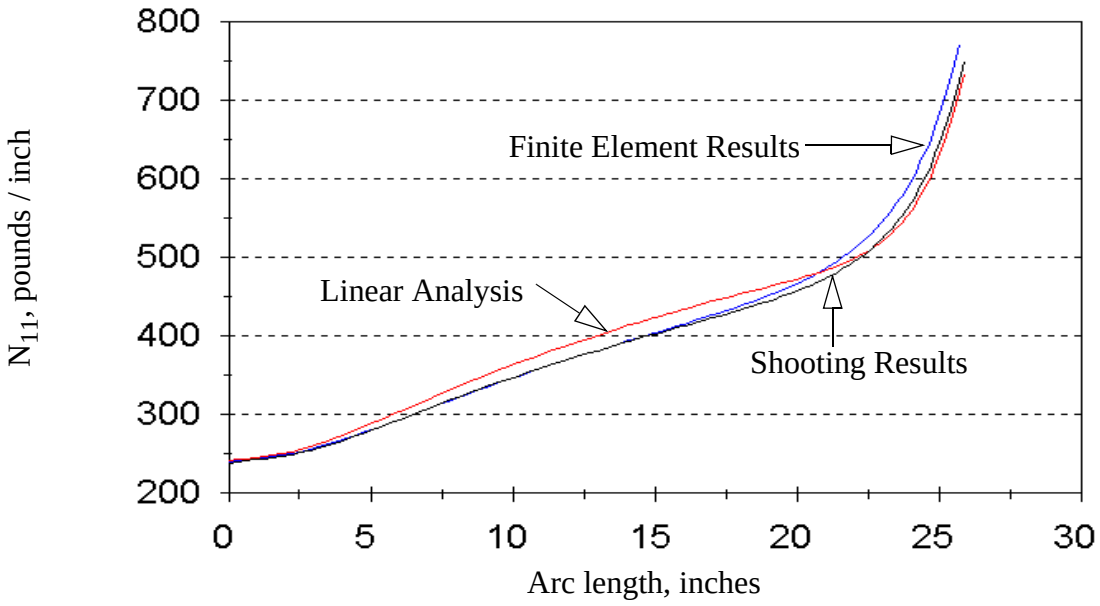

Fig. 5.29 Meridional Stress Resultant, Case IIIa

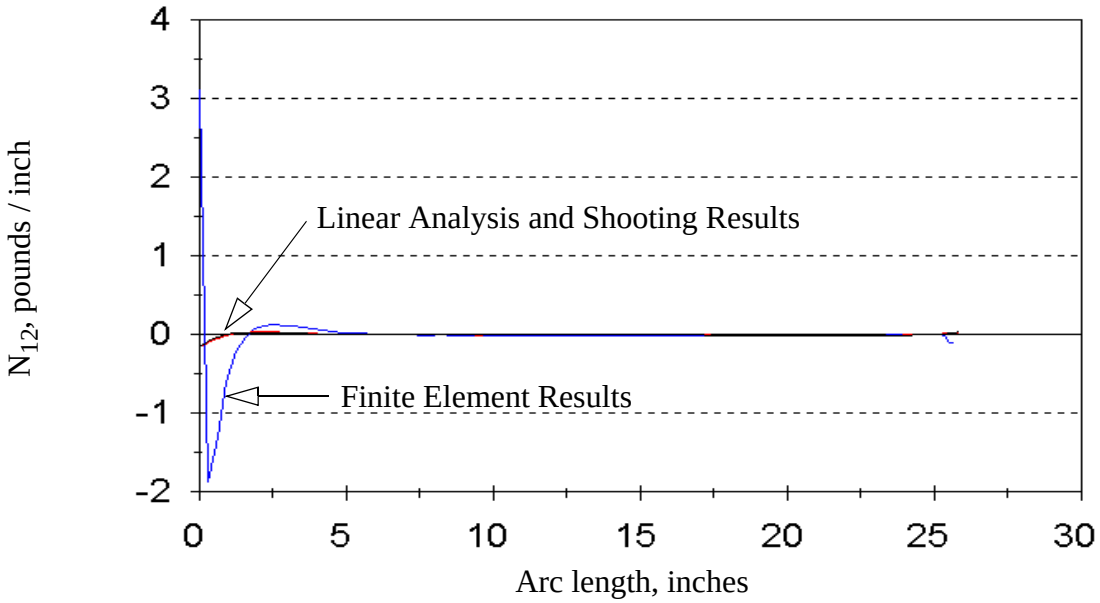

Fig. 5.30 In-plane Shear Stress Resultant, Case IIIa

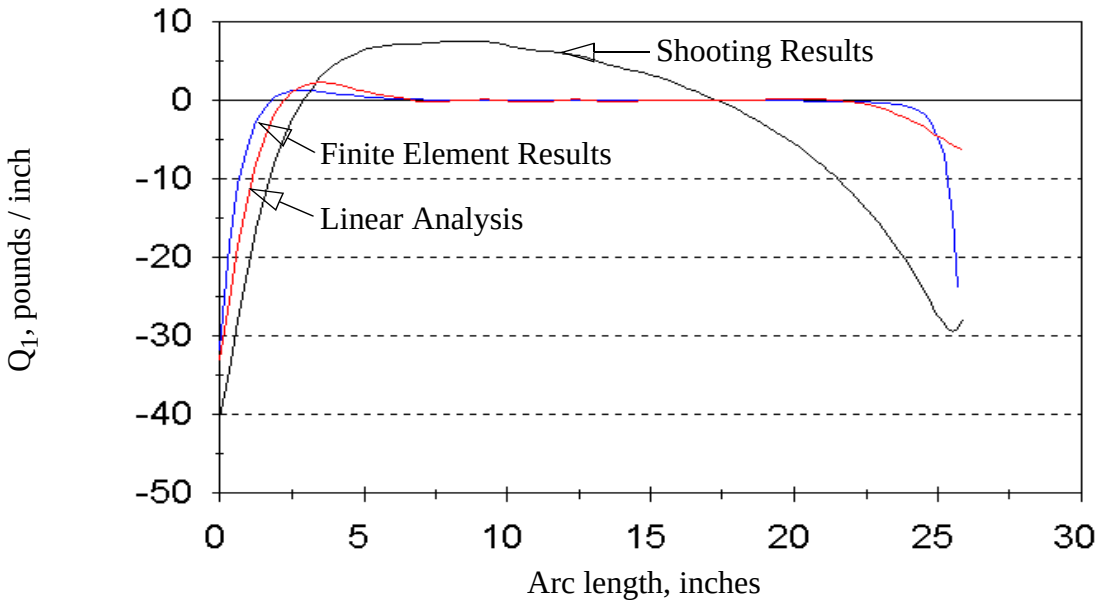

Fig. 5.31 Transverse Shear Stress Resultant on Meridional Face, Case IIIa

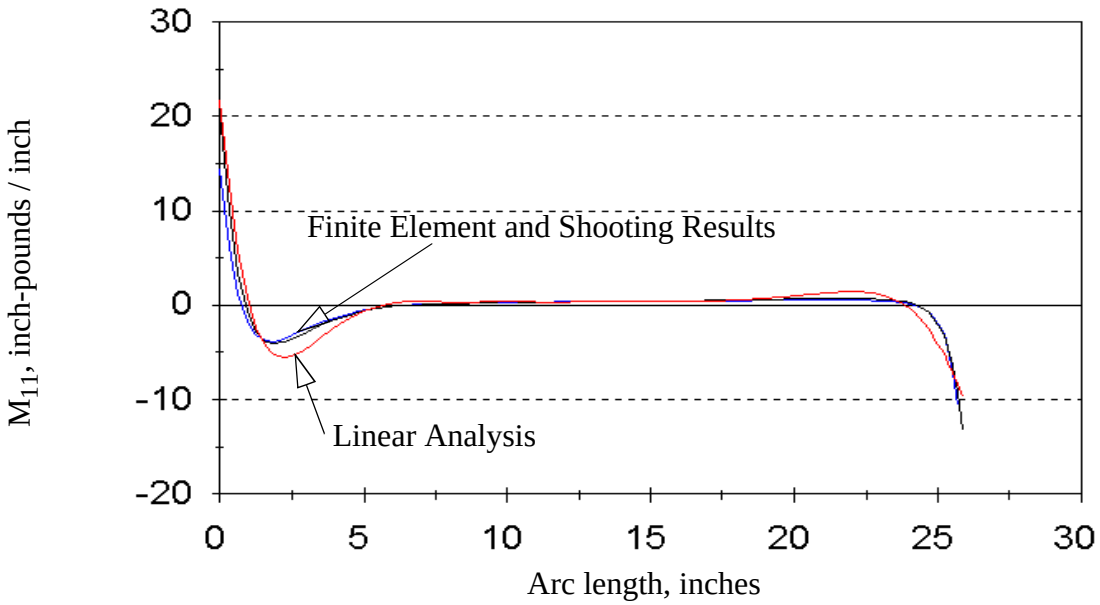

Fig. 5.32 Meridional Stress Couple, Case IIIa

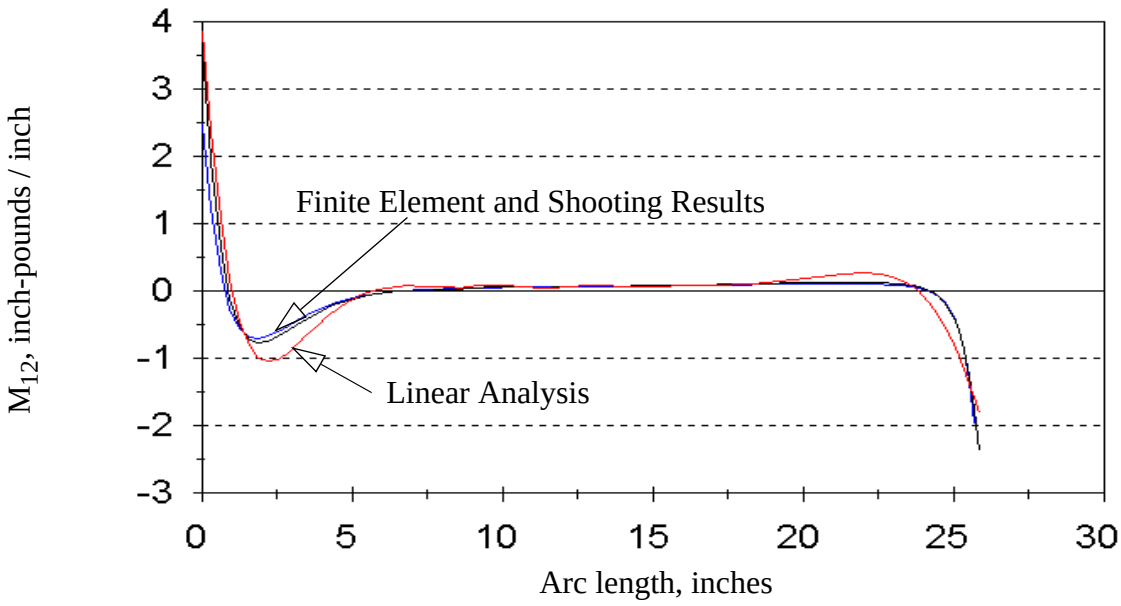

Fig. 5.33 In-plane Shear Stress Couple, Case IIIa

In performance of the verification tests for elliptical domes, a discrepancy was noted between the shooting analysis and the finite element analysis, for domes with a high degree of ellipticity. A representative sample showing this discrepancy is given below as Case IIIb. For this analysis, we continue to use a $[\pm 30_2]_s$ dome laminate, semi-major axis length of 24 inches, pressure of 60 psi and clamped end conditions, but with an ellipticity $e = 0.25$. This is a rather severe case of an ellipsoidal dome. The results presented here are for a geometrically linear analysis. The discrepancy noted is directly attributable to the use of a cubic spline interpolation for the geometry in the multiple shooting routine; changing the number and placement of the spline support points affects the waviness of the output of the shooting code. For this example, we have taken 11 support points, defining ten spline segments which each span 7.5 degrees of included angle. We have taken 10 shooting segments per spline segment. We thus have a set of 101 evenly spaced shooting points. With this mesh, the results of the two analyses (FEM and shooting) agree well for the following primary response variables: reference surface displacements *u*, *v*, *w*, ϕ_2 and resultants N_{11}, Q_1. Again, N_{12} from the two analyses disagree. The waviness shown in the following figures appears in association with the rotation ϕ_1, and all of the stress couples. The most egregious examples are depicted in Fig. 5.34.

5.5 Verification Case IV: Dome with internal ring stiffeners

For this final verification case, we examine the response of a stiffened, isotropic, spherical dome, with internal ring stiffeners. A similar test case has previously been published by Steinbrink and Johnson (1997). For that work, the finite element code ABAQUS was used as a benchmarking tool. For consistency, this last example is also analyzed using ABAQUS. The specifics of the problem are as follows: a linear analysis is performed for an isotropic spherical dome with clamped ends, under internal pressure. The dome is defined as having a six-inch radius, and thickness of 0.06 inches. Internal pressure of 20 psi is applied. Material properties are $E = 10.5 Msi$, $\nu = 0.33$, where E is the Young's modulus and ν is the Poisson's ratio of the dome material. Stiffening rings are defined to exist at the locations $\alpha = 20°, 40°, 60°$, with α as defined in Fig. 5.1. The rings have extensional stiffness of $E \cdot Area = 3.78(10^5)$ inch-pounds.

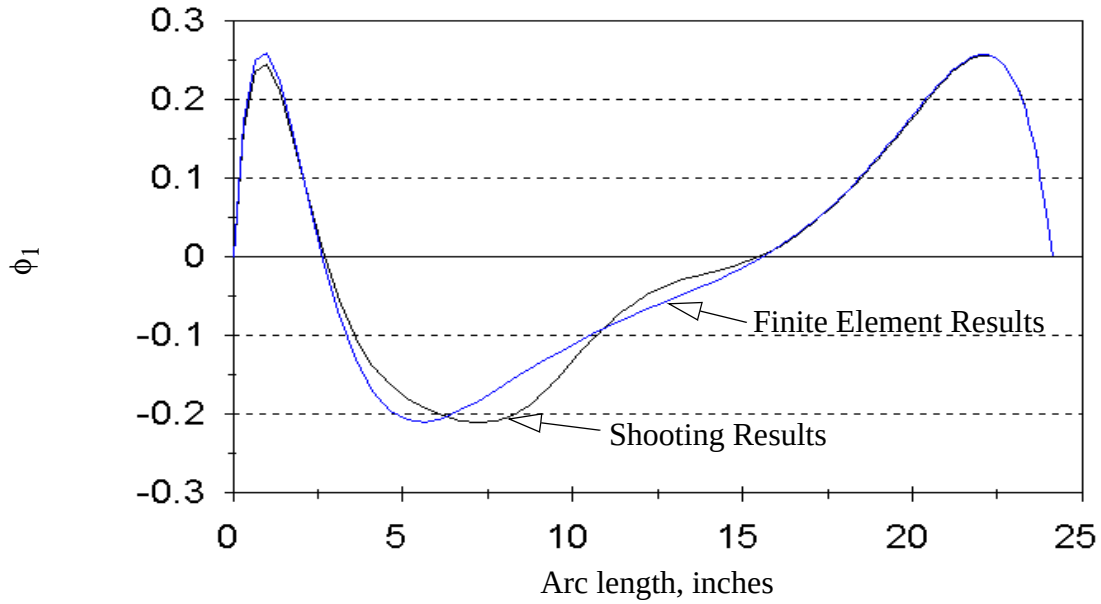

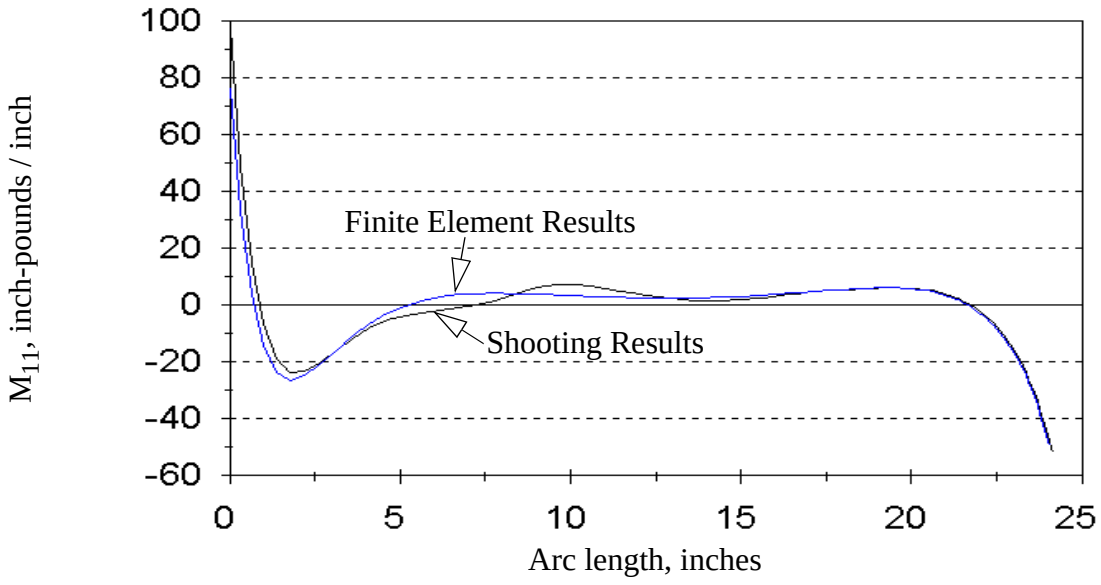

Fig. 5.34 Some Representative Results for Case IIIb

The dome is nearly hemispherical, with included angle in the range $0° \le \alpha \le 80°$. The finite element analysis utilizes 200 equally-sized SAX2 elements, a three-noded axisymmetric shell element; the shooting analysis uses 201 equally spaced shooting points, so that the two analyses cover the same mesh.

Of special interest in this case is the transverse shear stress resultant, Q_1, and it's derivative with respect to the arc length. It has previously been argued that the displacement-based finite element method has difficulty in prediction of the transverse shear stress resultant, and that accurate knowledge of both the transverse shear stress resultant and its derivative are desired for estimation of interlaminar stresses. This case, then, shows the utility of the current analysis method over the finite element method.

It may be seen by examination of Fig. 5.35 that the transverse shear stress resultant is adequately, though imperfectly, estimated by the finite element code. Indeed, one must look closely at the figure to see the difference between the results of the two analyses. On the other hand, the FEM analysis must be judged as wholly unsatisfactory for estimation of the gradient of the transverse shear stress resultant, shown in Fig. 5.36.

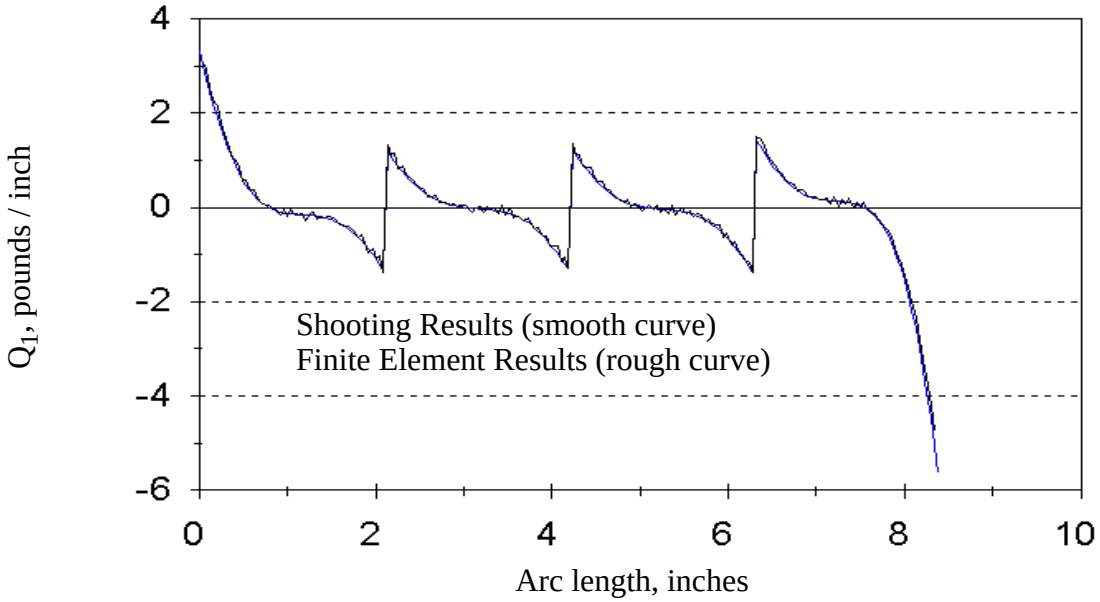

Fig. 5.35 Transverse Shear Stress Resultant, Case IV

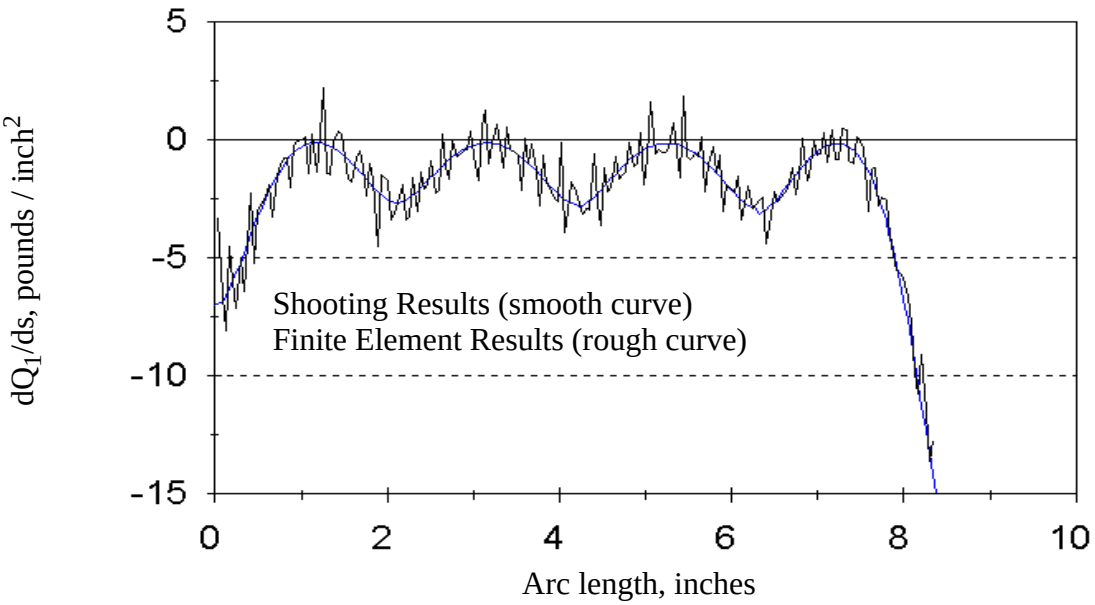

Fig. 5.36 Gradient of the Transverse Shear Stress Resultant, Case IV

In fairness, it should be noted that the results depicted in Fig. 5.36 are somewhat imprecise: the gradient attributed to the finite element analysis is not actually calculated by ABAQUS. The data for this curve are extracted from ABAQUS output using central differences, and smoothing out the "spikes" which occur at the stiffeners. The plotted results thus represent an attempt to derive more information than the finite element code was designed to give.